University Library

MINERVA ACCESS

A gateway to Melbourne's research publications

Minerva Access is the Institutional Repository of The University of Melbourne

Author/s:
Lin, Z;Zhou, J;Qu, Y;Pan, S;Han, Y;Lafleur, RPM;Chen, J;Cortez-Jugo, C;Richardson, JJ;Caruso, F

Title:
Luminescent Metal-Phenolic Networks for Multicolor Particle Labeling

Date:
2021-11-15

Citation:
Lin, Z., Zhou, J., Qu, Y., Pan, S., Han, Y., Lafleur, R. P. M., Chen, J., Cortez-Jugo, C., Richardson, J. J. & Caruso, F. (2021). Luminescent Metal-Phenolic Networks for Multicolor Particle Labeling. ANGEWANDTE CHEMIE-INTERNATIONAL EDITION, 60 (47), pp.24968-24975. https://doi.org/10.1002/anie.202108671.

Persistent Link:
https://hdl.handle.net/11343/290664

Check for updates

Author Manuscript

Title: Luminescent Metal–Phenolic Networks for Multicolor Particle Labeling

Authors: Zhixing Lin; Jiajing Zhou; Yijiao Qu; Shuaijun Pan; Yiyuan Han; René P. M. Lafleur; Jingqu Chen; Christina Cortez-Jugo; Joseph J. Richardson; Frank Caruso, Prof.

This is the author manuscript accepted for publication. It has not been through the copyediting, typesetting, pagination and proofreading process, which may lead to differences between this version and the Version of Record.

To be cited as: 10.1002/anie.202108671

Link to VoR: https://doi.org/10.1002/anie.202108671

Luminescent Metal–Phenolic Networks for Multicolor Particle Labeling

Zhixing Lin,[a] Jiajing Zhou,[a] Yijiao Qu,[a] Shuaijun Pan,[a] Yiyuan Han,[a] René P. M. Lafleur,[a] Jingqu Chen,[a] Christina Cortez-Jugo,[a] Joseph J. Richardson,[a] and Frank Caruso*[a]

[a] Z. Lin, Dr. J. Zhou, Y. Qu, Dr. S. Pan, Dr. Y. Han, Dr. R. P. M. Lafleur, J. Chen, Dr. C. Cortez-Jugo, Dr. J. J. Richardson, Prof. F. Caruso
ARC Centre of Excellence in Convergent Bio-Nano Science and Technology, and the Department of Chemical Engineering
The University of Melbourne
Parkville, Victoria 3010, Australia
E-mail: fcaruso@unimelb.edu.au

Supporting information for this article is given via a link at the end of the document.

Abstract: The development of fluorescence labeling techniques has attracted widespread interest in various fields, including biomedical science as it can facilitate high-resolution imaging and the spatiotemporal understanding of various biological processes. We herein report a supramolecular fluorescence labeling strategy using luminescent metal–phenolic networks (MPNs) constructed from metal ions, phenolic ligands, and common and commercially available dye molecules. The rapid labeling process (<5 min) produces ultrathin coatings (~10 nm) on diverse particles (e.g., organic, inorganic, and biological entities) with customized luminescence (e.g., red, blue, multichromatic, and white light) simply through the selection of fluorophores. The fluorescent coatings are stable at pH from 1 to 8 and in complex biological media owing to the dominant π interactions between the dyes and MPNs. These coatings exhibit negligible cytotoxicity and their strong fluorescence is retained even when internalized into intracellular compartments. This supramolecular fluorescence labeling strategy is expected to provide a versatile approach for fluorescence labeling with potential in diverse fields across the physical and life sciences, including materials science and biomedicine.

Introduction

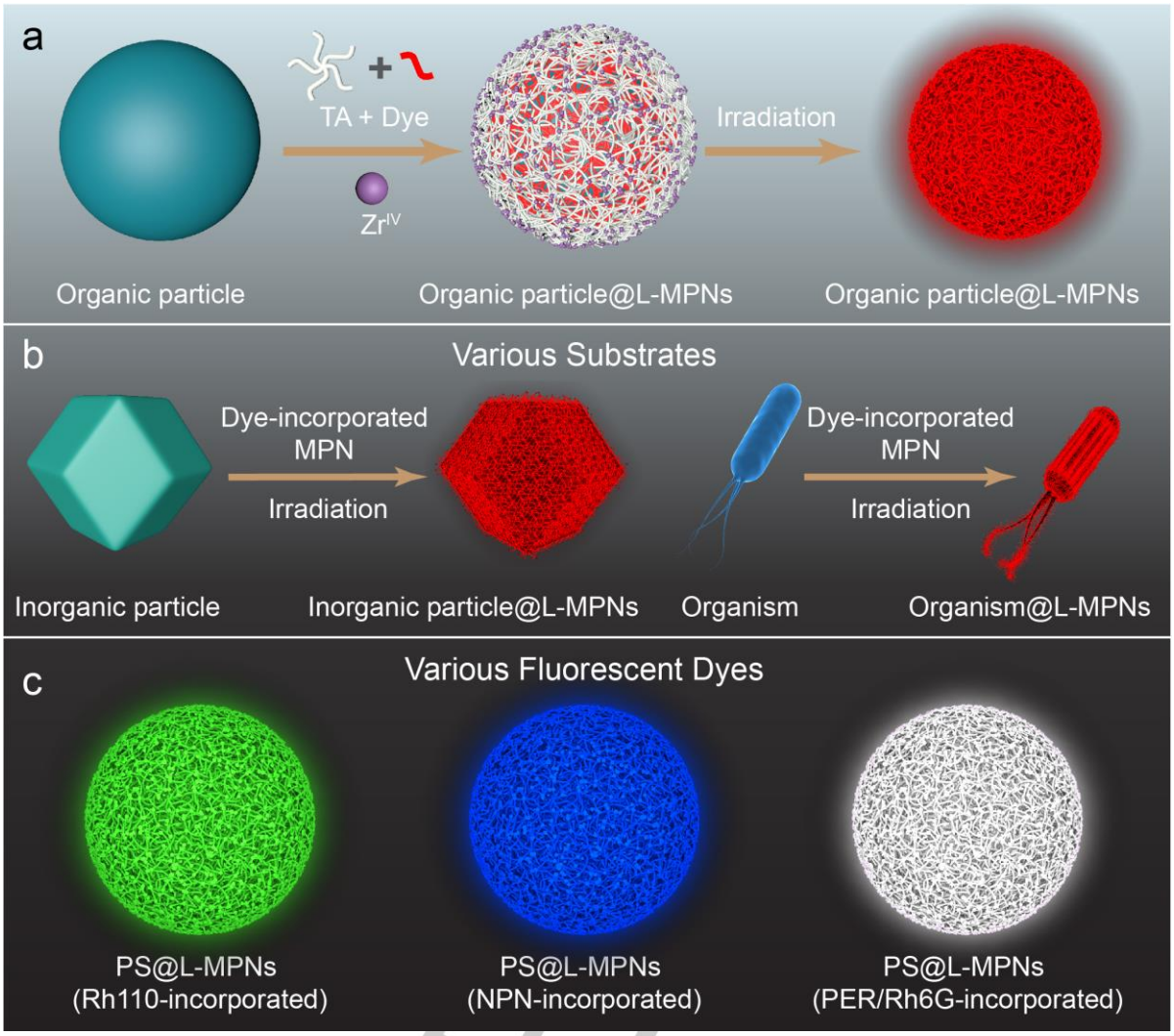
Fluorescent particles play a pivotal role in a variety of applications including bioimaging, optical sensing, and tissue engineering.[1] A wide range of fluorescent particles have been synthesized and they can be classified into two broad categories: (i) particles that are inherently fluorescent, including quantum dots,[2] carbon-based dots,[3] upconversion nanoparticles,[4] aggregation-induced emission nanoparticles,[5] and (ii) particles that require labeling with fluorophores, including fluorescently doped silica nanoparticles,[6] and fluorophore-conjugated metal nanoparticles,[7] lipids,[8] and polymers.[9] Fluorophore particle labeling can be achieved via the encapsulation of fluorophores or fluorophore-conjugated molecules during particle formation or the encoding of fluorescence in nonfluorescent (preformed) particle systems. The latter approach is widely used, as it can provide flexibility and opportunities for multimodal or multifunctional sensing.[10] However, it typically requires the covalent attachment of fluorophore molecules onto the surface of particles, which often necessitates specialized conjugation chemistries, along with specific surface chemistries of the particles (e.g., isothiocyanate at a specific pH for amine-functionalized surfaces). Alternatively, fluorophores can be incorporated into the particles (i.e., in the core volume),[11] although this approach requires porous or swellable particles, thus limiting the range of particles that can be used. In addition, the formation of fluorescent coatings[12] has been widely studied but this generally requires either covalent pre- or post-labeling of the coating material, which in general is achieved either through covalent or noncovalent bonding, thus requiring certain chemistries on the particles and/or fluorophore choice. A further issue can be the leaching of the fluorescent dye when noncovalent interactions are used for particle labeling (e.g., in biological fluids).[13] Therefore, there is a need for the development of a modular and general protocol applicable for a broad range of particle types and that can endow the particles with robust fluorescence properties in diverse conditions (e.g., various pH and biological media).

Luminescent crystalline metal–organic frameworks have attracted interest owing to their strong emission and broad luminescence characteristics that originate from various emission sources (e.g., organic ligands, metal ions, metal clusters, and metal–ligand charge transfer).[14] Moreover, it was recently demonstrated that porous crystalline metal–organic frameworks can load high quantities of guest molecules, including fluorescent dyes, which can provide greater compositional flexibility for designing fluorescent probes without being limited to emissive ligands or metal ions that can change the structure or morphology of the probe itself.[15] Thus, the availability of a wide selection of commercially available dyes can endow metal–organic frameworks with emission across the full visible light spectrum (from 380 to 700 nm) and polychromatic light emission (e.g., white light) with high brightness.[15a,15e,15f] Although luminescent crystalline metal–organic frameworks have found application as sensors and light-emitting diodes,[16] studies on their potential for particle surface engineering have been limited owing to the relatively poor affinity of crystalline metal–organic frameworks to substrates.[17]

In contrast, metal–phenolic networks (MPNs), an amorphous class of metal–organic materials that are composed of metals and phenolic molecules, can be deposited on a wide range of

Author Manuscript

This article is protected by copyright. All rights reserved



Scheme 1. (a) Schematic of the deposition of L-MPNs on a particle (particle@L-MPNs) and its subsequent fluorescence. (b) Assembly of L-MPNs on various substrates, including organic and inorganic, and biological entities. (c) Schematic representation of tunable light emission of particles by integrating different dyes inside the MPNs: Rh110, rhodamine 110 chloride; NPN, *N*-phenyl-1-naphthylamine; PER, perylene; and Rh6G, rhodamine 6G.

surfaces owing to the high adherence of polyphenols.[18] Moreover, phenolics can interact with materials via hydrogen bonds without compromising their ability to participate in π interactions, which has enabled the use of MPNs for engineering particle systems for various applications.[19] Based on the abundance of aromatic rings in common dyes, we hypothesized that integrating MPNs with organic dyes through π interactions would result in diverse luminescent metal–organic frameworks via a simple and versatile coating process.

Herein, we report a versatile and robust supramolecular fluorescence strategy to label particles of different compositions, sizes, and surface chemistries with luminescent MPNs (L-MPNs, Scheme 1). Specifically, polyphenols (e.g., tannic acid, TA) and fluorescent dyes (e.g., rhodamine B, RhB) (Figures S1 and S2) were first mixed to form complexes via π interactions in aqueous environments, and metal ions (e.g., Zr^{IV}) were subsequently added to assemble the complexes into conformal coatings on diverse substrates (e.g., particle@L-MPNs). L-MPN coating refers to TA–RhB–Zr^{IV} coating unless a different polyphenol–dye–metal ion combination is specified. We demonstrate the integration of 8 representative dyes on 16 representative inorganic, organic, and biological substrates (Table S1). Customized luminescence (e.g., red, blue, multichromatic, and white light) was readily achieved using common and simple fluorophores without the need for covalent conjugation or specialized surface chemistry modifications to the substrates. Moreover, the obtained luminescent particles exhibited negligible cytotoxicity and high stability in several biological environments (e.g., phosphate-buffered saline (PBS), Dulbecco's modified Eagle's medium (DMEM) with 10% fetal bovine serum (FBS)). In addition, the fluorescently labeled particles were used to study cell association and internalization in real time. This supramolecular fluorescence labeling strategy is versatile and facile, as it can be completed using readily available equipment and reagents. Our study not only provides an avenue for the rapid fluorescence labeling of particles, but also expands the potential applications of MPN-based materials.

Results and Discussion

This article is protected by copyright. All rights reserved

Author Manuscript

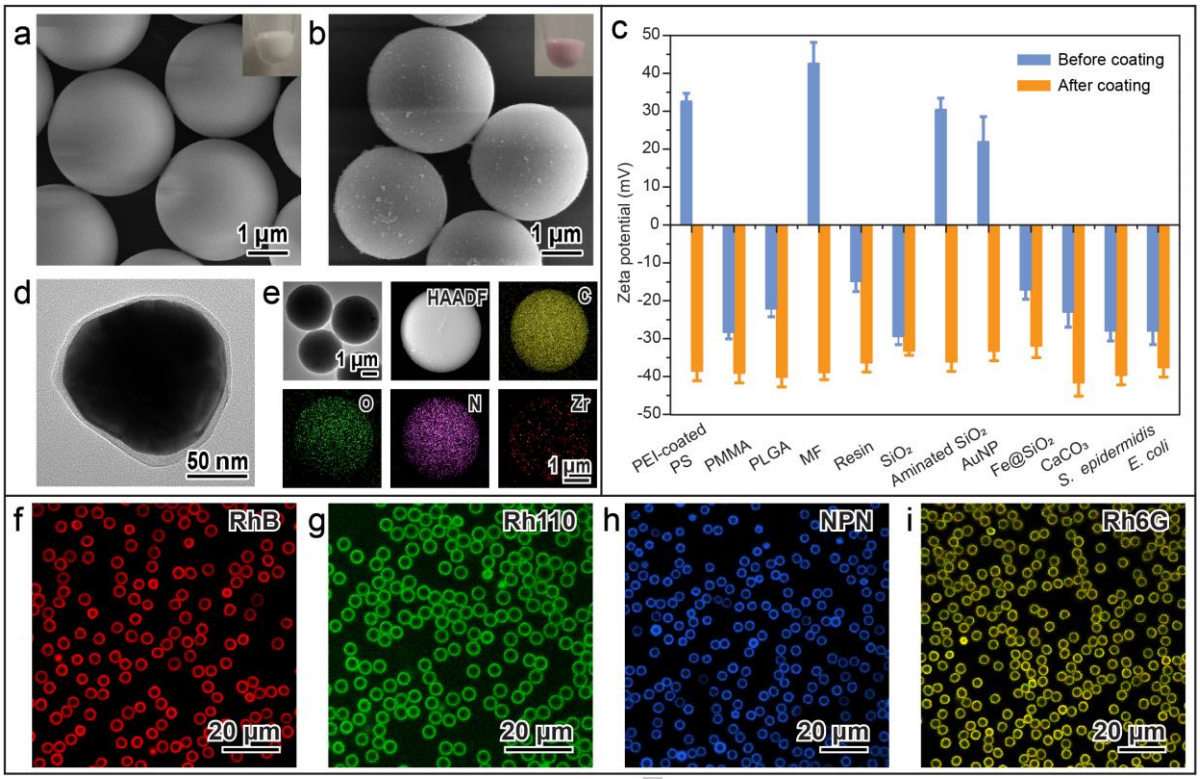


Figure 1. Assembly of L-MPNs on various substrates. (a, b) SEM images of PS particles before (a) and after (b) L-MPN coating. Insets are the corresponding photographs of the particle dispersion before and after coating. (c) Zeta potential values of diverse particles in water before and after L-MPN coating. The error bars represent standard deviations (n = 3). (d) Transmission electron microscopy (TEM) image of a AuNP@L-MPN particle, with a thin L-MPN coating. (e) TEM, HAADF, and EDX elemental mapping of the PS@L-MPN particles. (f–i) Assembly of L-MPNs on PS particles with different dyes: RhB (f), Rh110 (g), NPN (h), and Rh6G (i).

The assembly of L-MPNs on polystyrene (PS) planar and particulate substrates was first examined. Briefly, the model phenolic molecule and fluorophore, TA (6 mM) and RhB (0.096 mM), respectively, were added to the PS planar substrate or PS template suspension to form TA–RhB complexes (Figure S3) in solution and on the PS substrates. Zr^{IV} was then added and the pH was raised, followed by mixing at ambient temperature to cross-link the TA–RhB complexes by metal coordination. Finally, any free unbound dye and MPN complexes were removed by washing. The Zr^{IV}–TA network was selected because of its high stability under various pH and thermal conditions,[20] as well as its transparency, which is expected to have minimal effect on the luminescence of the dyes (Figure S4). The color of the planar and particulate substrates turned pink after coating (Figures 1a,b and S4), and the surface of the particles became rougher, as observed by scanning electron microscopy (SEM, Figure 1a,b), confirming the presence of the L-MPN coating on the substrate. It is notable that negligible fluorescence was observed on particles when they were labeled with only TA and RhB, suggesting the essential role of the coordination networks for successful fluorescence labeling (Figure S5). The formation of L-MPNs shifted the surface zeta potential of the PS particles from –26 to –40 mV due to the deprotonation of TA (Figure S6). The choice of dye did not significantly alter the surface charge of the L-MPN coating owing to the small fraction of dye (less than 18 mol%) (Figure S7). The strong surface charge after coating is expected to improve colloidal stability owing to increased interparticle electrostatic repulsion, and negligible aggregation was observed after coating (Figure S8).[21] The thickness of the L-MPN coating was around 10 nm, and it can be increased by repeating the L-MPN deposition cycle (e.g., around 55 nm after 5 coating cycles; Figure S9).

To demonstrate the versatility of this strategy, fluorescence labeling of 16 different types of particle substrates with distinct physicochemical properties (e.g., composition, size, and surface chemistry) was examined. Specifically, PS, polyethyleneimine (PEI)-coated PS, poly(methyl methacrylate) (PMMA), poly(lactic-*co*-glycolic acid) (PLGA), melamine formaldehyde (MF), resin, gold nanoparticle (AuNP), SiO_2, aminated SiO_2, Fe@SiO_2, $CaCO_3$, *Staphylococcus epidermidis* (*S. epidermidis*), and *Escherichia coli* (*E. coli*) were successfully coated as confirmed by the shift in the zeta potential value after coating (Figure 1c) and by confocal laser scanning microscopy (CLSM, Figures S10 and S11). High-angle annular dark field (HAADF) and energy-dispersive X-ray (EDX) mapping demonstrated the presence of N (from the (RhB) dye) and Zr on the PS template (Figure 1e). Cross-sectional CLSM images of a fluorescently labeled resin particle demonstrated uniform fluorescence on the surface of the particles (Figure S12). Importantly, the luminescence color of the L-MPN coatings can be tuned over a wide emission range according to the chosen dye (Figure 1f–i). For example, red, green, blue, and yellow fluorescence was encoded in PS particles by using RhB, Rh110, NPN, and Rh6G, respectively. Collectively, these results indicate that this labeling strategy can generate a range of emission profiles on diverse substrates across length scales from 150 nm to 1 cm.

Author Manuscript

This article is protected by copyright. All rights reserved

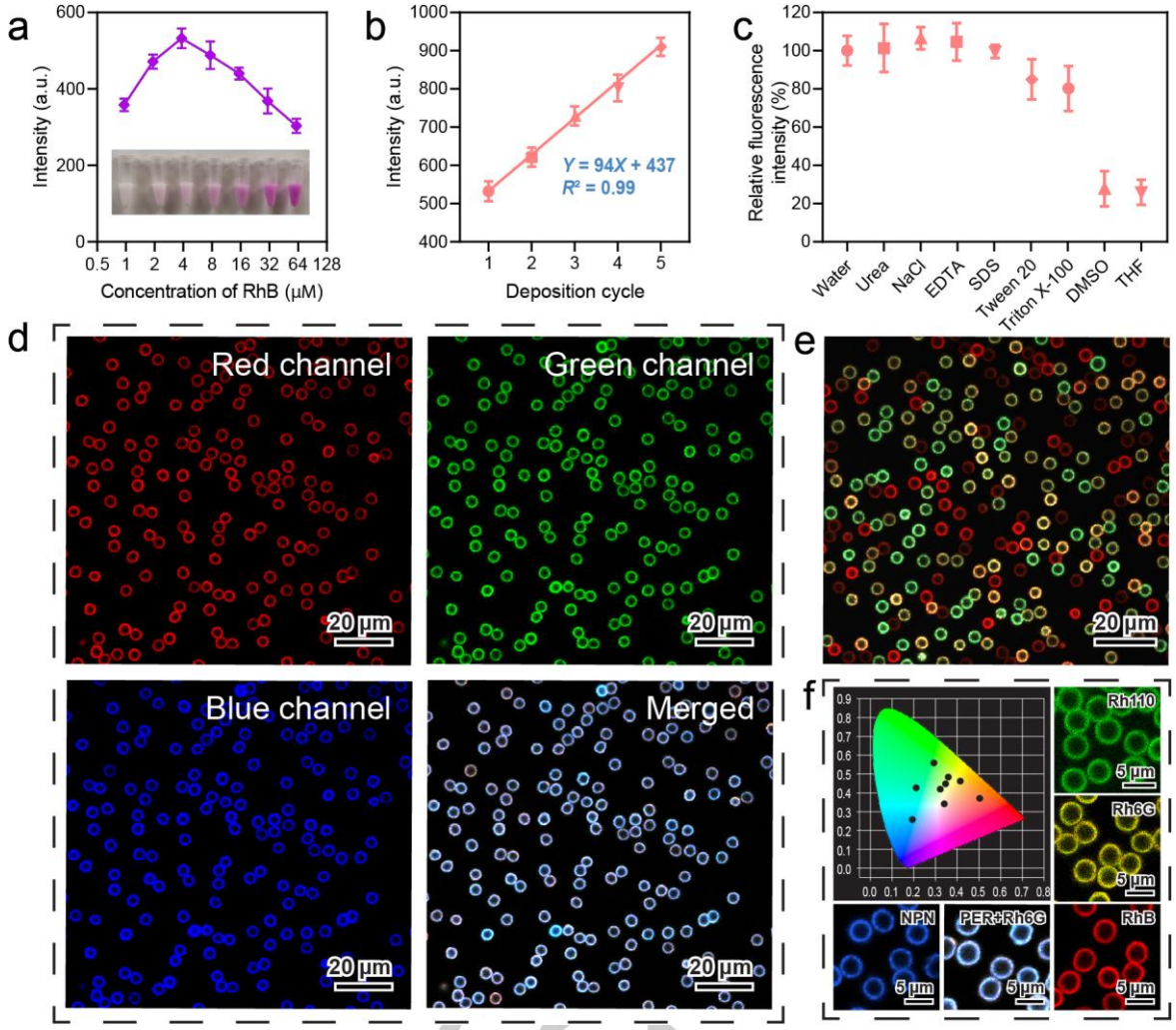


Figure 2. (a) Fluorescence intensity of dispersions of L-MPN particles labeled with different concentrations of RhB. (b) Fluorescence intensity of L-MPN particles prepared using different numbers of deposition cycles. (c) Relative fluorescence intensity of SiO_2@L-MPN particles after incubation in various media and resuspended in water. The error bars represent standard deviations (n = 3). (d) CLSM images showing the multichromatic emission of L-MPNs particles co-labeled with PER and Rh6G. (e) CLSM images of a mixture of L-MPNs with different emission colors. (f) CIE chromaticity coordinates of different L-MPN-labeled particles. EDTA, ethylenediaminetetraacetic acid; SDS, sodium dodecyl sulfate; DMSO, dimethyl sulfoxide; THF, terahydrofuran.

Flow cytometry revealed that the labeled PS particles (3.35 μm in diameter) had a narrow fluorescence distribution (Figure S13). The fluorescence intensity of the particles was varied by tuning the initial concentration of RhB from 0.96 to 61.44 μM, while keeping the concentrations of TA (0.24 mM) and Zr^{IV} (0.24 mM) fixed (Figure 2a and S14). Specifically, the fluorescence intensity initially increased with an increase in RhB concentration, and then decreased when the RhB concentration was above 3.84 μM, which can be attributed to aggregation-induced fluorescence quenching with higher ratios of nonfluorescent H-type dimers instead of fluorescent monomers.[22] Nevertheless, as observed in the CLSM images, the coated particles displayed strong fluorescence at all the concentrations examined (Figure S15). The fluorescence intensity of the particles was also increased simply by repeating the coating procedure, where the fluorescence intensity increased by approximately 18% in each deposition cycle after the initial coating (Figure 2b and S16). Owing to the strong interaction between RhB and MPNs and the likely aggregation of dyes on the surface of the particles, the fluorescence emission wavelength red-shifted from 576 nm for free RhB to 587 nm for PS@L-MPN (prepared with RhB) particles (Figure S17a). The quantum yields of the PS@L-MPN particles prepared with RhB and Rh6G were 9.8 and 30.4%, respectively (Figure S17), which are both ~30% of that of the free dyes (which are not incorporated into MPNs). In contrast, the photostability of the dyes integrated with MPNs was higher than that of the free dye upon irradiation at room temperature (Figure S18).[23]

We then investigated the assembly and stabilizing mechanisms of the L-MPN coatings using various characterization methods. Fourier transform infrared spectroscopy analysis showed a reduced intensity of the HO−C stretching peak in L-MPNs when compared with the absorption stretching band in TA at 3304 cm^{-1}, suggesting the coordination of phenolic groups with metal ions (Figure S19). The interaction between RhB and the MPN was further explored using hydrophobic competitors (e.g., Tween 20, Triton X-100, sodium dodecyl sulfate (SDS)), a hydrogen bond competitor (e.g., urea), an ionic competitor (e.g., NaCl), and π competitors (e.g., tetrahydrofuran (THF) and dimethyl sulfoxide (DMSO)).[19a,24] The SiO_2@L-MPN particles were incubated in these solutions for 24 h, and then centrifuged

This article is protected by copyright. All rights reserved

Author Manuscript

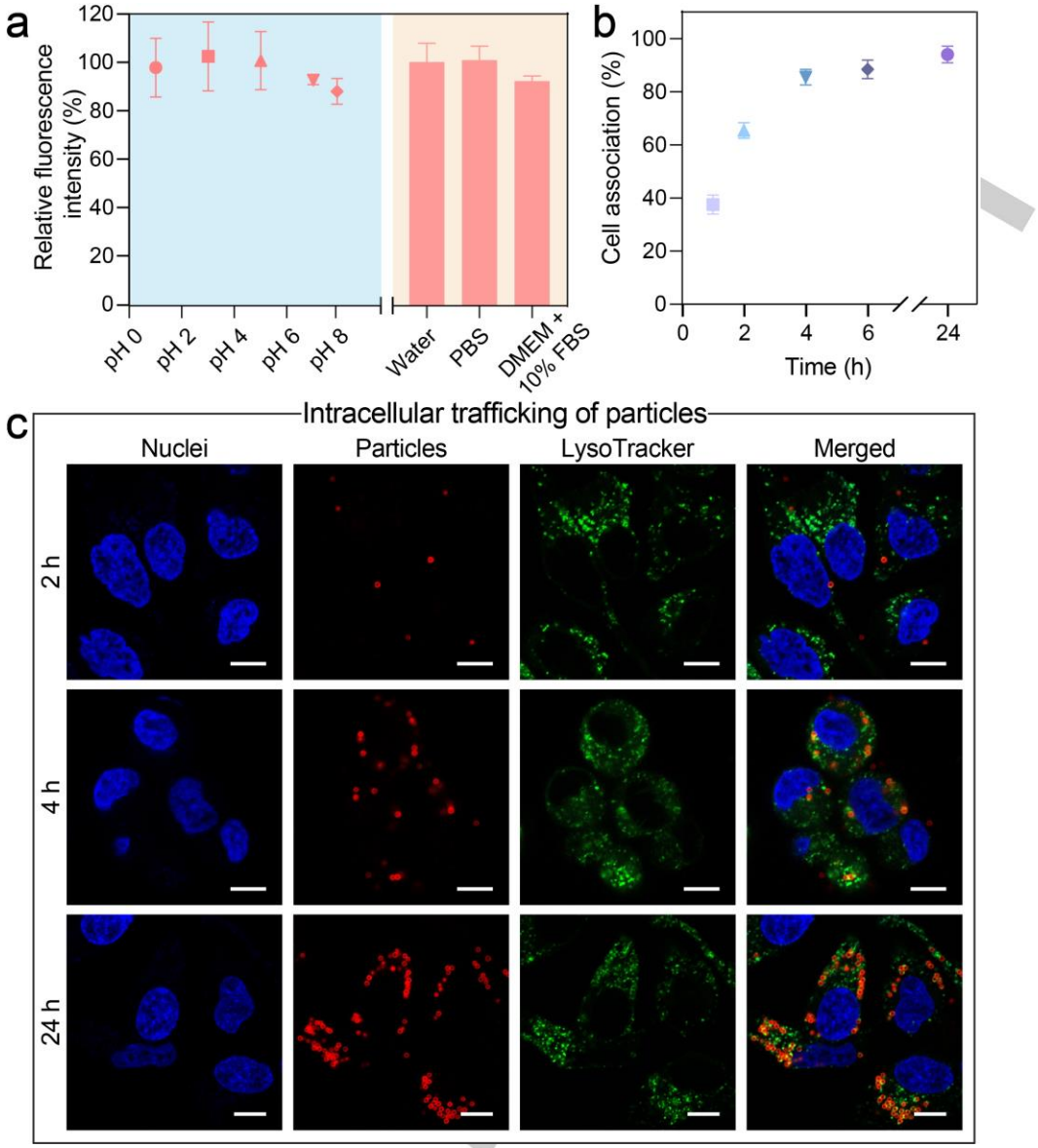


Figure 3. (a) Fluorescence stability of PMMA@L-MPN particles at different pH and in different culture media after incubation for 24 h. (b) Quantitative cell association results of PMMA@L-MPN particles incubated with HeLa cells at 37 °C for different times. The error bars represent standard deviations (n = 3). (c) CLSM images of the intracellular delivery of PMMA@L-MPN particles in HeLa cells. Scale bars are 10 μm. The nuclei (blue) were stained with Hoechst 33342, and the endosomes/lysosomes (green) were stained with LysoTracker Green.

and redispersed in water to monitor the residual fluorescence of the labeled particles. It is noted that the sizes of the fluorescent dyes (M_w < 1 kDa) relative to the pore size of the MPNs (permeable to dextrans with M_w ~500 kDa[18d]) are relatively small and therefore any dye leaching or dye fluorescence changes are unlikely caused by any alterations in the pore size of MPNs even when interaction competitors (e.g., SDS, Tween 20) are present. The fluorescence of the particles was stable in 100 mM Tween 20, Triton X-100, SDS, urea, and NaCl but significantly decreased in the organic solvents examined (Figure 2c), which suggests that π interactions (e.g., cation–π and π–π) are the dominant interactions between RhB and the MPN.[19a,25] Furthermore, all-atom molecular dynamics simulations have demonstrated that π interactions are dominant between polyphenols and other aromatic molecules.[19a]

In addition, MPN capsules could be prepared by removing the PS cores in THF (Figure S20). When MPN coatings were formed on $CaCO_3$ templates, ethylenediaminetetraacetic acid was used to dissolve the cores to obtain L-MPN capsules (Figure S21). Notably, the $CaCO_3$-templated MPN capsules retained their fluorescence, which further validated the presence of the dye–polyphenol complexes in the coating rather than their incorporation in the template particles.

Furthermore, L-MPN coatings containing different metal ions (e.g., Fe^{III}, Al^{III}) and polyphenols (e.g., epigallocatechin gallate) were prepared, demonstrating compositional flexibility (and subsequent functionality flexibility) of the coatings (Figure S22). For example, Fe^{III}–TA-based L-MPNs (with RhB) were not fluorescent (quenched) under basic environments because of the broad spectrum light absorption of Fe^{III}–TA[18d] complexes but became fluorescent in acidic environments because of the

This article is protected by copyright. All rights reserved

Author Manuscript

reduced light absorption of Fe^{III}–TA allowing for enhanced excitation of the dyes and hence emission from the films. In addition, such a pH change can potentially alter the redox potential of L-MPNs (e.g., at low pH) (Figure S23).[18a,26] This property may be used for intracellular pH sensing, which is of interest for early disease diagnosis.[27] In addition, emissive metal ions (e.g., lanthanum metal ions) can be used to construct L-MPNs via the incorporation of attenuating co-ligands (e.g., acetylacetone).[28] Considering the wide availability of metal ions and functional polyphenols (e.g., anticancer and antibacterial phenolics), the present MPN-mediated labeling strategy holds potential for generating multifunctional particles that could potentially be used simultaneously for imaging and therapeutic applications.[29]

Luminescent materials with multiple excitation/emission peaks have also attracted interest owing to their promise for a range of applications, such as light-emitting diodes, anticounterfeiting, and information storage.[27,30] Therefore, the present L-MPN labeling approach was extended to include multiple dyes to tune the excitation/emission spectra of the labeled particles. For example, high-quality white color was achieved by fabricating a bi-layer L-MPN with separate PER (i.e., green and blue fluorescence colors) and Rh6G (i.e., green and red fluorescence colors) L-MPN layers (Figure 2d). By assembling L-MPNs with different or combinations of commercial dyes, we created a library of L-MPNs with different emission spectra and diverse CIE chromaticity coordinates (Figures 2e,f and S24).[30] Compared to several reported labeling techniques, our strategy is versatile and rapid, as it can be completed without the assistance of specialized equipment in under 5 min, and produces ultrathin fluorescent coatings (~10 nm) on substrates of diverse size and surface chemistry, where the emission spectra can be easily tuned through the choice of fluorophore(s) (Table S2).

Fluorescence imaging is widely used for studying various biomedical applications such as intracellular catalysis, drug delivery, and biodistribution.[31] In a typical biomedical scenario, particles are first exposed to extracellular fluids (pH ≈7.4) and then undergo intracellular uptake (e.g., endosomal pH 5.5–6.0; lysosomal pH 4.5–5.0).[32] To validate the reliability of the present L-MPN labeling for biomedical studies (specifically the use of L-MPNs for fluorescence tracking to monitor the fate of particles), we first examined the stability of PMMA@L-MPN particles in various pH conditions and cell culture media. The fluorescence remained stable over a pH range of 1–8 and in various media (i.e., PBS, DMEM supplied with 10% FBS) after 24 h of incubation (Figure 3a), which also demonstrates the negligible leaching of dyes from L-MPNs owing to their robust π interactions.[19a] We next examined the cytotoxicity of the PMMA@L-MPN particles by incubating the L-MPN particles with HeLa cells at different particle-to-cell ratios. HeLa cells were chosen as model cancer cells for in vitro cell imaging. The labeled particles showed negligible cytotoxicity to cells even at high particle-to-cell ratios (~5000:1, Figure S25a), likely because of the use of natural building blocks (i.e., TA). The labeled particles also showed negligible cytotoxicity to the macrophage cell line Raw 264.7 (Figure S25b).

The fluorescence of the labeled particles was further exploited for studying cell association and internalization of particles in real time. As observed from Figure 3b, cell association reached a plateau around 85% after the particles were incubated with cells for 4 h (Figure 3b). Internalization was visualized by CLSM as a function of incubation time (i.e., 2, 4, and 24 h), where association, internalization, and trafficking were observed (Figure 3c). Moreover, the red fluorescence of the particles remained intact throughout the incubation, demonstrating the photostability of the coatings inside different cellular compartments. Importantly, the particles outside the cell did not interact with the nucleus (blue) or endosome (green) labeling kits, suggesting that the L-MPN coatings are not compromised by external interfering fluorescent molecules (Figure S26). The endosomal staining revealed that the particles were internalized via endocytosis (Figure S27), which is typical for most particles of this size (1.36 μm).

Conclusion

In summary, we developed a facile and versatile supramolecular fluorescence labeling strategy using L-MPNs constructed from metal ions, phenolic ligands, and dye molecules. Sixteen representative types of particle substrates with different compositions, sizes, and surface chemistries were successfully labeled. Customized luminescence (e.g., red, blue, multichromatic, and white light) was achieved by choosing from a broad selection of dyes without needing to consider the chemical composition owing to the supramolecular nature of MPNs. The fluorescent coating is stable in many biological environments, such as serum and cytosol, further validating its potential in studying the cell association and internalization of particles in real time. Considering the wide availability of metal ions, functional polyphenols (e.g., anticancer and antibacterial phenolics), and commercially available dyes, we expect that this versatile fluorescence labeling strategy will open up new applications for luminescent coatings and provide an alternative for the modular design of a broader palette of hybrid imaging probes.

Acknowledgements

This research was conducted and funded by the Australian Research Council Centre of Excellence in Convergent Bio-Nano Science and Technology (project number CE140100036). F.C. acknowledges the award of a National Health and Medical Research Council Senior Principal Research Fellowship (GNT1135806). R.P.M.L. acknowledges the Netherlands Organisation for Scientific Research for a Rubicon postdoctoral fellowship (project 019.182EN.034). J.J.R. acknowledges JSPS KAKENHI Grant Number 20F20373 and JSPS Fellowship P20373. This work was performed in part at the Materials Characterisation and Fabrication Platform, Biosciences Microscopy Unit, and Ian Holmes Imaging Centre, Bio21 Institute at The University of Melbourne, and the Victorian Node of the Australian National Fabrication Facility. The authors acknowledge Yingjie Hu, Jiaying Song, and Sukhvir Kaur Bhangu for helpful discussions.

This article is protected by copyright. All rights reserved

Author Manuscript

Keywords: luminescent metal–organic frameworks • polyphenols • self-assembly • supramolecular chemistry • surface engineering

[1] a) H.-B. Cheng, Y. Li, B. Z. Tang, J. Yoon, *Chem. Soc. Rev.* **2020**, *49*, 21–31; b) F. W. Pratiwi, C. W. Kuo, B.-C. Chen, P. Chen, *Nanomedicine* **2019**, *14*, 1759–1769; c) Y. Zhao, H. Zeng, X.-W. Zhu, W. Lu, D. Li, *Chem. Soc. Rev.* **2021**, *50*, 4484–4531; d) A. B. Chinen, C. M. Guan, J. R. Ferrer, S. N. Barnaby, T. J. Merkel, C. A. Mirkin, *Chem. Rev.* **2015**, *115*, 10530–10574; e) J. Yao, M. Yang, Y. Duan, *Chem. Rev.* **2014**, *114*, 6130–6178; f) O. S. Wolfbeis, *Chem. Soc. Rev.* **2015**, *44*, 4743–4768.

[2] a) L. Du, N. A. Nosratabad, Z. Jin, C. Zhang, S. Wang, B. Chen, H. Mattoussi, *J. Am. Chem. Soc.* **2021**, *143*, 1873–1884; b) D. A. Hanifi, N. D. Bronstein, B. A. Koscher, Z. Nett, J. K. Swabeck, K. Takano, A. M. Schwartzberg, L. Maserati, K. Vandewal, van de Y. Burgt, Y. v. d. Burgt, A. Salleo, A. P. Alivisatos, *Science* **2019**, *363*, 1199–1202; c) H. Utzat, W. Sun, A. E. Kaplan, F. Krieg, M. Ginterseder, B. Spokoyny, N. D. Klein, K. E. Shulenberger, C. F. Perkinson, M. V. Kovalenko, M. G. Bawendi, *Science* **2019**, *363*, 1068–1072; d) C. R. Kagan, C. B. Murray, *Nat. Nanotechnol.* **2015**, *10*, 1013–1026; e) A. M. Smith, S. Nie, *J. Am. Chem. Soc.* **2011**, *133*, 24–26.

[3] a) K. Nekoueian, M. Amiri, M. Sillanpää, F. Marken, R. Boukherroub, S. Szunerits, *Chem. Soc. Rev.* **2019**, *48*, 4281–4316; b) B. K. Walther, C. Z. Dinu, D. M. Guldi, V. G. Sergeyev, S. E. Creager, J. P. Cooke, A. Guiseppi-Elie, *Mater. Today* **2020**, *39*, 23–46.

[4] a) Q. Liu, Y. Zhang, C. S. Peng, T. Yang, L.-M. Joubert, S. Chu, *Nat. Photonics* **2018**, *12*, 548–553; b) S. Chen, A. Z. Weitemier, X. Zeng, L. He, X. Wang, Y. Tao, A. J. Huang, Y. Hashimotodani, M. Kano, H. Iwasaki, L. K. Parajuli, S. Okabe, D. B. L. Teh, A. H. All, I. Tsutsui-Kimura, K. F. Tanaka, X. Liu, T. J. McHugh, *Science* **2018**, *359*, 679–684; c) X. Li, F. Zhang, D. Zhao, *Chem. Soc. Rev.* **2015**, *44*, 1346–1378; d) N. J. Johnson, A. Korinek, C. Dong, F. C. J. M. van Veggel, *J. Am. Chem. Soc.* **2012**, *134*, 11068–11071.

[5] a) J. Li, J. Wang, H. Li, N. Song, D. Wang, B. Z. Tang, *Chem. Soc. Rev.* **2020**, *49*, 1144–1172; b) C. Liu, X. Wang, J. Liu, Q. Yue, S. Chen, J. W. Lam, L. Luo, B. Z. Tang, *Adv. Mater.* **2020**, *32*, 2004685.

[6] a) J. A. Erstling, J. A. Hinckley, N. Bag, J. Hersh, G. B. Feuer, R. Lee, H. F. Malarkey, F. Yu, K. Ma, B. A. Baird, U. B. Wiesner, *Adv. Mater.* **2021**, *33*, e2006829; b) F. Chen, B. Madajewski, K. Ma, D. K. Zanoni, H. Stambuk, M. Z. Turker, S. Monette, L. Zhang, B. Yoo, P. Chen, R. J. C. Meester, S. d. Jonge, P. Montero, E. Phillips, T. P. Quinn, M. Gönen, S. Sequeira, E. d. Stanchina, P. Zanzonic, U. Wiesner, S. G. Patel, M. S. Bradbury, *Sci. Adv.* **2019**, *5*, eaax5208.

[7] a) M. Yang, P. Moroz, Z. Jin, D. S. Budkina, N. Sundrani, D. Porotnikov, J. Cassidy, Y. Sugiyama, A. N. Tarnovsky, H. Mattoussi, M. Zamkov, *J. Am. Chem. Soc.* **2019**, *141*, 11286–11297; b) B. Kim, G. Han, B. J. Toley, C.-k. Kim, V. M. Rotello, N. S. Forbes, *Nat. Nanotechnol.* **2010**, *5*, 465–472.

[8] a) M. H. Cheng, K. M. Harmatys, D. M. Charron, J. Chen, G. Zheng, *Angew. Chem. Int. Ed.* **2019**, *58*, 13394–13399; *Angew. Chem.* **2019**, *131*, 13528; b) X. Cai, D. Mao, C. Wang, D. Kong, X. Cheng, B. Liu, *Angew. Chem. Int. Ed.* **2018**, *57*, 16396–16400; *Angew. Chem.* **2018**, *130*, 16634.

[9] a) Y. Ju, H. G. Kelly, L. F. Dagley, A. Reynaldi, T. E. Schlub, S. K. Spall, C. A. Bell, J. Cui, A. J. Mitchell, Z. Lin, A. K. Wheatley, K. J. Thurecht, M. P. Davenport, A. I. Webb, F. Caruso, S. J. Kent, *ACS Nano* **2020**, *14*, 15723–15737; b) L. Su, R. Li, S. Khan, R. Clanton, F. Zhang, Y.-N. Lin, Y. Song, H. Wang, J. Fan, S. Hernandez, A. S. Butters, G. Akabani, R. MacLoughlin, J. Smolen, K. L. Wooley, *J. Am. Chem. Soc.* **2018**, *140*, 1438–1446.

[10] a) M. Yang, Y. Liu, X. Jiang, *Chem. Soc. Rev.* **2019**, *48*, 850–884; b) K. Shin, J. W. Choi, G. Ko, S. Baik, D. Kim, O. K. Park, K. Lee, H. R. Cho, S. I. Han, S. H. Lee, D. J. Lee, N. Lee, H.-C. Kim, T. Hyeon, *Nat. Commun.* **2017**, *8*, 15807; c) Q. Yue, Y. Zhang, Y. Jiang, J. Li, H. Zhang, C. Yu, A. A. Elzatahry, A. Alghamdi, Y. Deng, D. Zhao, *J. Am. Chem. Soc.* **2017**, *139*, 4954–4961; d) B. J. Battersby, D. Bryant, W. Meutermans, D. Matthews, M. L. Smythe, M. Trau, *J. Am. Chem. Soc.* **2000**, *122*, 2138–2139; e) C. I. Olariu, H. H. Yiu, L. Bouffier, T. Nedjadi, E. Costello, S. R. Williams, C. M. Halloran, M. J. Rosseinsky, *J. Mater. Chem.* **2011**, *21*, 12650–12659.

[11] a) M. Liu, X. Zheng, V. Grebe, D. J. Pine, M. Weck, *Nat. Mater.* **2020**, *19*, 1354–1361; b) F. Hu, C. Zeng, R. Long, Y. Miao, L. Wei, Q. Xu, W. Min, *Nat. Methods* **2018**, *15*, 194–200; c) S. Tang, Y. Zhang, P. Dhakal, L. Ravelo, C. L. Anderson, K. M. Collins, F. M. Raymo, *J. Am. Chem. Soc.* **2018**, *140*, 4485–4488; d) F. Zhang, Q. Shi, Y. Zhang, Y. Shi, K. Ding, D. Zhao, G. D. Stucky, *Adv. Mater.* **2011**, *23*, 3775–3779; e) M. Han, X. Gao, J. Z. Su, S. Nie, *Nat. Biotechnol.* **2001**, *19*, 631–635.

[12] a) F. C. Lin, J. I. Zink, *J. Am. Chem. Soc.* **2020**, *142*, 5212–5220; b) J. Luan, A. Seth, R. Gupta, Z. Wang, P. Rathi, S. Cao, H. G. Derami, R. Tang, B. Xu, S. Achilefu, J. J. Morrissey, S. Singamaneni, *Nat. Biomed. Eng.* **2020**, *4*, 518–530; c) J. H. Li, P. Santos-Otte, B. Au, J. Rentsch, S. Block, H. Ewers, *Nat. Commun.* **2020**, *11*, 4259; d) M. Olszyna, A. Debrassi, C. Üzüm, L. Dähne, *Adv. Funct. Mater.* **2019**, *29*, 1805998.

[13] a) L. De Smet, G. Vancoillie, P. Minshall, K. Lava, I. Steyaert, E. Schoolaert, E. Van De Walle, P. Dubruel, K. De Clerck, R. Hoogenboom, *Nat. Commun.* **2018**, *9*, 1123; b) J. Yu, C. Wu, X. Zhang, F. Ye, M. E. Gallina, Y. Rong, I. C. Wu, W. Sun, Y. H. Chan, D. T. Chiu, *Adv. Mater.* **2012**, *24*, 3498–3504; c) A. Reisch, A. S. Klymchenko, *Small* **2016**, *12*, 1968–1992.

[14] a) T. Y. Luo, P. Das, D. L. White, C. Liu, A. Star, N. L. Rosi, *J. Am. Chem. Soc.* **2020**, *142*, 2897–2904; b) J. Cornelio, T. Y. Zhou, A. Alkas, S. G. Telfer, *J. Am. Chem. Soc.* **2018**, *140*, 15470–15476; c) W. J. Newsome, S. Ayad, J. Cordova, E. W. Reinheimer, A. D. Campiglia, J. K. Harper, K. Hanson, F. J. Uribe-Romo, *J. Am. Chem. Soc.* **2019**, *141*, 11298–11303; d) M. D. Allendorf, C. A. Bauer, R. K. Bhakta, R. J. T. Houk, *Chem. Soc. Rev.* **2009**, *38*, 1330–1352; e) Y. Cui, Y. Yue, G. Qian, B. Chen, *Chem. Rev.* **2012**, *112*, 1126–1162.

[15] a) X. Y. Liu, K. Xing, Y. Li, C. K. Tsung, J. Li, *J. Am. Chem. Soc.* **2019**, *141*, 14807–14813; b) V. Glembockyte, M. Frenette, C. Mottillo, A. M. Durantini, J. Gostick, V. Strukil, T. Friscic, G. Cosa, *J. Am. Chem. Soc.* **2018**, *140*, 16882–16887; c) Z. Yuan, L. Zhang, S. Li, W. Zhang, M. Lu, Y. Pan, X. Xie, L. Huang, W. Huang, *J. Am. Chem. Soc.* **2018**, *140*, 15507–15515; d) Y. Wen, T. Sheng, X. Zhu, C. Zhuo, S. Su, H. Li, S. Hu, Q. L. Zhu, X. Wu, *Adv. Mater.* **2017**, *29*, 1700778; e) J. Yu, Y. Cui, H. Xu, Y. Yang, Z. Wang, B. Chen, G. Qian, *Nat. Commun.* **2013**, *4*, 2719; f) C. Y. Sun, X. L. Wang, X. Zhang, C. Qin, P. Li, Z. M. Su, D. X. Zhu, G. G. Shan, K. Z. Shao, H. Wu, J. Li, *Nat. Commun.* **2013**, *4*, 2717; g) J. Deng, K. Wang, M. Wang, P. Yu, L. Mao, *J. Am. Chem. Soc.* **2017**, *139*, 5877–5882.

[16] a) W. P. Lustig, S. Mukherjee, N. D. Rudd, A. V. Desai, J. Li, S. K. Ghosh, *Chem. Soc. Rev.* **2017**, *46*, 3242–3285; b) Z. Hu, B. J. Deibert, J. Li, *Chem. Soc. Rev.* **2014**, *43*, 5815–5840; c) Y. Cui, Y. Yue, G. Qian, B. Chen, *Chem. Rev.* **2012**, *112*, 1126–1162.

[17] C. Jo, H. J. Lee, M. Oh, *Adv. Mater.* **2011**, *23*, 1716–1719.

[18] a) Z. Lin, J. Zhou, C. Cortez-Jugo, Y. Han, Y. Ma, S. Pan, E. Hanssen, J. J. Richardson, F. Caruso, *J. Am. Chem. Soc.* **2020**, *142*, 335–341; b) S. Pan, E. Goudeli, J. Chen, Z. Lin, Q.-Z. Zhong, W. Zhang, H. Yu, R. Guo, J. J. Richardson, F. Caruso, *Angew. Chem. Int. Ed.* **2021**, *60*, 14586–14594; *Angew. Chem.* **2021**, *133*, 14707–14715; c) J. Guo, B. L. Tardy, A. J. Christofferson, Y. Dai, J. J. Richardson, W. Zhu, M. Hu, Y. Ju, J. Cui, R. R. Dagastine, I. Yarovsky, F. Caruso, *Nat. Nanotechnol.* **2016**, *11*, 1105–1111; d) H. Ejima, J. J. Richardson, K. Liang, J. P. Best, M. P. van Koeverden, G. K. Such, J. Cui, F. Caruso, *Science* **2013**, *341*, 154–157

[19] a) J. Zhou, Z. Lin, M. Penna, S. Pan, Y. Ju, S. Li, Y. Han, J. Chen, G. Lin, J. J. Richardson, I. Yarovsky, F. Caruso, *Nat. Commun.* **2020**, *11*, 4804; b) J. Zhou, Z. Lin, Y. Ju, M. A. Rahim, J. J. Richardson, F. Caruso, *Acc. Chem. Res.* **2020**, *53*, 1269–1278; c) D. Wu, J. Zhou, M. N. Creyer, W. Yim, Z. Chen, P. B. Messersmith, J. V. Jokerst, *Chem. Soc. Rev.* **2021**, *50*, 4432–4483.

[20] M. A. Rahim, G. Lin, P. P. Tomanin, Y. Ju, A. Barlow, M. Bjornmalm, F. Caruso, *ACS Appl. Mater. Interfaces* **2020**, *12*, 3746–3754.

[21] A. S. Dukhin, P. J. Goetz, *Colloids Surf., A* **1998**, *144*, 49–58.

[22] F. L. Arbeloa, P. R. Ojeda, I. L. Arbeloa, *J. Lumin.* **1989**, *44*, 105–112.

[23] a) S. K. Bhangu, G. Bocchinfuso, M. Ashokkumar, F. Cavalieri, *Nanoscale Horiz.* **2020**, *5*, 553–563; b) Z. Fan, L. Sun, Y. Huang, Y. Wang, M. Zhang, *Nat. Nanotechnol.* **2016**, *11*, 388–394; c) H. Giloh, J. W. Sedat, *Science* **1982**, *217*, 1252–1255.

This article is protected by copyright. All rights reserved

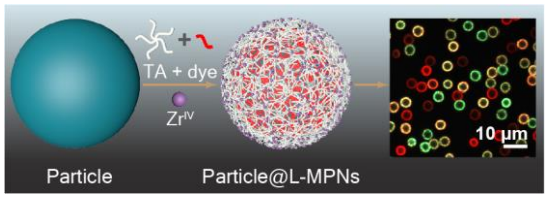
Author Manuscript

[24] J. E. Chung, S. Tan, S. J. Gao, N. Yongvongsoontorn, S. H. Kim, J. H. Lee, H. S. Choi, H. Yano, L. Zhuo, M. Kurisawa, J. Y. Ying, *Nat. Nanotechnol.* **2014**, *9*, 907–912.
[25] S. Kim, J. Huang, Y. Lee, S. Dutta, H. Y. Yoo, Y. M. Jung, Y. Jho, H. Zeng, D. S. Hwang, *Proc. Natl. Acad. Sci. U. S. A.* **2016**, *113*, E847–E853.
[26] a) T. Liu, W. Liu, M. Zhang, W. Yu, F. Gao, C. Li, S. B. Wang, J. Feng, X. Z. Zhang, *ACS Nano* **2018**, *12*, 12181–12192; b) Q.-Z. Zhong, S. Pan, M. A. Rahim, G. Yun, J. Li, Y. Ju, Z. Lin, Y. Han, Y. Ma, J. J. Richardson, F. Caruso, *ACS Appl. Mater. Interfaces* **2018**, *10*, 33721–33729.
[27] G. Lan, K. Ni, E. You, M. Wang, A. Culbert, X. Jiang, W. Lin, *J. Am. Chem. Soc.* **2019**, *141*, 18964–18969.
[28] J. Guo, Y. Ping, H. Ejima, K. Alt, M. Meissner, J. J. Richardson, Y. Yan, K. Peter, D. Von Elverfeldt, C. E. Hagemeyer, F. Caruso, *Angew. Chem. Int. Ed.* **2014**, *53*, 5546–5551; *Angew. Chem.* **2014**, *126*, 5652–5657.
[29] S. K. Sun, H. F. Wang, X. P. Yan, *Acc. Chem. Res.* **2018**, *51*, 1131–1143.
[30] H. Q. Yin, X. B. Yin, *Acc. Chem. Res.* **2020**, *53*, 485–495.
[31] M. E. Davis, D. M. Shin, *Nat. Rev. Drug Discovery* **2008**, *7*, 771–783.
[32] J. R. Casey, S. Grinstein, J. Orlowski, *Nat. Rev. Mol. Cell Biol.* **2010**, *11*, 50–61.

WILEY-VCH
Author Manuscript

This article is protected by copyright. All rights reserved

Entry for the Table of Contents



A supramolecular fluorescence labeling strategy is established using luminescent metal–phenolic networks constructed from metal ions, phenolic ligands, and dye molecules. Tunable and customized luminescence (e.g., red, blue, multichromatic, and white light) is achieved on inorganic, organic, and biological substrates, with potential applications in the physical and life sciences.

WILEY-VCH
Author Manuscript

This article is protected by copyright. All rights reserved